


Secondary electron emission in the scattering of fast probes by metallic interfaces

Alberto Rivacoba *

Materials Physics Center CSIC-UPV/EHU, Donostia International Physics Center DIPC,
Paseo Manuel Lardizabal 4, 20018 Donostia-San Sebastian, Spain

 (Received 9 June 2022; revised 3 December 2022; accepted 19 December 2022; published 4 January 2023)

In the frame of a nonretarded local density hydrodynamic approach nonlocal effects in the scattering of a fast probe interacting with a metallic interface are studied. In addition to quantal effects in the electron-gas response, effects derived from the interface density profile are taken into account. The relevance in the excitation spectrum of both collective and single electron excitations is studied. For probes at grazing incidence the decay of collective excitations into single electron ones is found. Around the surface plasmon frequency the momentum carried by these excitations allows identifying them as secondary electrons emerging from the target. The recoil associated with them leads to a repulsive force with qualitative agreement with experimental observations. Effects of the momentum transfer in the deflection angle of the beam are also studied.

DOI: [10.1103/PhysRevB.107.035401](https://doi.org/10.1103/PhysRevB.107.035401)

I. INTRODUCTION

The use of the local dielectric theory (LDT) to the study of the energy loss experienced by fast probes interacting with condensed matter was first proposed by Fermi [1] and extended to deal with interfaces by Ritchie [2]. LDT has been widely applied in electron energy-loss spectroscopy (EELS) in scanning transmission electron microscopy, (STEM) where the use of experimentally measured optical dielectric data, as well the development of powerful computational methods [3–5] has opened the application of this approach to the analysis of the loss spectra in a wide range of materials and to targets of increasingly complexity [6,7] with good qualitative and quantitative agreement with the experiments.

The success of the dielectric approach to explain the longitudinal momentum transfer, the physical magnitude defining the probe energy loss, encouraged to extend this theory to calculate the transverse component of the momentum transfer (TMT) experimentally found by Cowley in STEM experiments [8]. In this case the so calculated deflection was about three orders of magnitude smaller than the experimental one [9–11]. More recently the experimental evidence of the ability of the STEM beam to control the motion of nanoparticles [12–14] has renewed the interest on this topic [7,15–19].

The difference in the suitability of the LDT to describe correctly transversal and longitudinal components of the momentum transfer is an obvious consequence of the drastic simplification of the polarizability model posed by the local approach where the response of the medium does not depend on the wave-vector \mathbf{k} of the exciting field. In the interaction with interfaces the relevance of the contribution of the large wave vectors to the probe scattering can be better understood by writing the medium response in terms of the induced charge density $\rho(\mathbf{k}, \omega)$. Let us consider a probe

moving with velocity $\mathbf{v} = v\mathbf{u}_z$, parallel to a interface with impact parameter b [as shown in the inset of Fig. 1(a)]. Assuming the probe velocity to be constant, the induced charge density can be written as $\rho(\mathbf{k}, \omega) = \tilde{\rho}(k_x, Q, \omega)\delta(k_z - \omega v^{-1})$, where $Q = [k_y^2 + (\omega/v)^2]^{1/2}$ and the components of the momentum transfer $\Delta\mathbf{p}$ (per unit path length) can be written as

$$\frac{\Delta p_z}{\Delta z} = \frac{1}{\pi^3 v^3} \int_0^\infty \omega d\omega \int_0^\infty dk_y \int_{-\infty}^\infty dk_x \frac{1}{k^2} \times \text{Im}[\tilde{\rho}(k_x, Q, \omega)e^{ik_x b}], \quad (1)$$

$$\frac{\Delta p_x}{\Delta z} = \frac{1}{\pi^3 v^2} \int_0^\infty d\omega \int_0^\infty dk_y \int_{-\infty}^\infty dk_x \frac{k_x}{k^2} \times \text{Im}[\tilde{\rho}(k_x, Q, \omega)e^{ik_x b}], \quad (2)$$

where $k^2 = k_x^2 + k_y^2 + \omega^2 v^{-2}$ [21].

Equation (1) shows that the relevant contribution to the stopping power basically arises from the small values of k_x , given that the contribution of large values is severely damped both by the fast oscillating phase $e^{ik_x b}$ as well by the k_x^2 dependence of the denominator. It explains the fact that a sound description of the polarizability at small \mathbf{k} as that provided by the liquid-crystal display technology, leads to reasonably accurate loss spectra, even at grazing incidence.

Nevertheless, in Eq. (2), the contribution of large k_x components to the factor k_x/k^2 fades out more slowly so that at grazing incidence those values provide a relevant contribution to the TMT. Therefore, for grazing probes, a thorough description of the interface response to large values of the transverse momentum is needed. This description should take into account quantal effects of the electron gas as well those derived from interface density profile.

There have been many theoretical approaches to implement quantal corrections to the polarizability of the target.

*alberto.rivacoba@ehu.eus

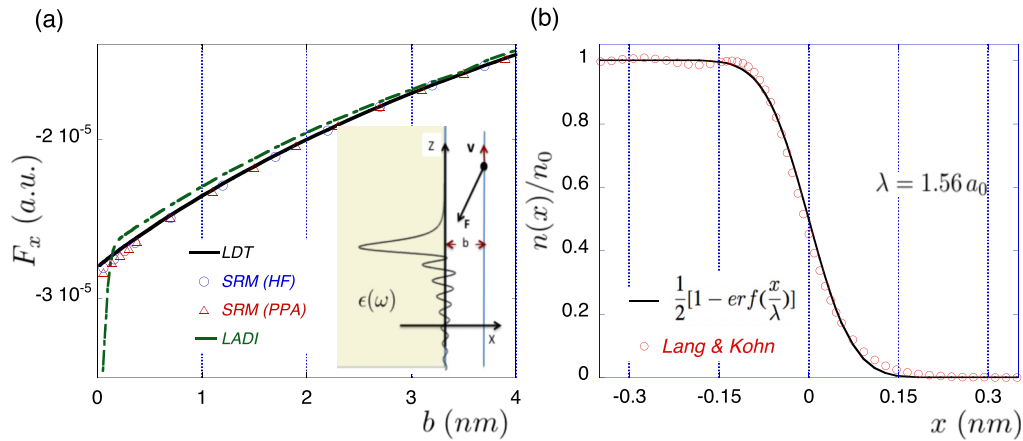


FIG. 1. (a) Transverse component of the force experienced by a 100-keV electron moving parallel to an Al interface with different dielectric functions. Continuous line (LDT), circles and triangles correspond to a sharp interface characterized by local Drude, hydrodynamic (SRM HF) and plasmon pole (SRM PPA) dielectric functions, respectively. The plot labeled as LADI corresponds to the solution of a Poisson equation in a diffuse interface with the density profile shown in (b) [see (a)]. The inset in (a) schematically represents the interaction of the probe with the surface wake. (b) Profile of the unperturbed charge density normalized to the bulk value n_0 . Red circles (\circ) and the black line, respectively, correspond to Table I ($r_s = 2a_0$) of Ref. [20] and to the fit used in this paper. Parameters of the dielectric functions: $\hbar\omega_p = 15.3$ eV, $\beta^2 = 0.49$ a.u., and $\hbar\gamma = 1$ eV.

Rigorous *ab initio* calculations based on the *Time-dependent density-functional theory* have been applied to study the optical response of nanoparticles [22–25] or its effects on EELS [26]. The main drawback of this method lies in its computational demand, that, in practice, reduces its applicability to nanoparticles consisting of several hundreds of atoms. A more efficient computational strategy to tackle surface nonlocal effects consists of the use of the unperturbed ground-state electron density of the target $n_0(\mathbf{r})$ as an input and then consider the interaction with the probe as a perturbation, described by a set of macroscopic parameters. One of these approaches, based on the *surface-response functions* (SRFs) describes the polarizability of the medium in terms of a couple of ω -dependent parameters, the so-called *Feibelman parameters* [27,28]. *Hydrodynamic models* (HDs) have been also developed to calculate the charge density induced by the exciting field, in terms just of one parameter, the unperturbed charge density of the target $n_0(\mathbf{r})$, the quantal effects being given by the corresponding *local pressure coefficient* $\beta(\mathbf{r})$ [21,29].

Both approaches, SRF and HD usually extend the range of the \mathbf{k} dependence of the polarizability up to k^2 corrections in the dielectric response of the electron gas. Nevertheless, they are unable to describe the phenomena associated with large momentum transfer, such as the electron-hole and single electron (SE) excitations. These excitations can be formally introduced into the theory by the use of an appropriate local dielectric function $\epsilon(\mathbf{k}, \omega)$; the suitability of this approach will be analyzed in the next section.

The aim of this paper is study the role of large momentum excitations in the scattering of fast probes by metallic interfaces, putting the emphasis on their contribution to TMT. For that purpose we have reformulated the hydrodynamic model of Ref. [21] where the response of a nonabrupt interface to a fast probe was studied by extending the momentum response of the polarizability to account for k^4 contributions. In Sec. I, we study the limitations of the different

dielectric approaches for the study of TMT, and then (Sec. II) we present a new HD formulation able to reproduce electron-hole and single electron excitations. Finally in Sec. III we present the results of this theory. As an Appendix the local approach to a nonabrupt interface to study the TMT is also presented.

Atomic units (a.u.) are used throughout in the theoretical expressions. In the plots lengths and energies are given in nanometers and electronvolts. The definition of the functions defining the electron-gas parameters along the interface has been made clear by adding a tilde over them: so, for instance, $\tilde{\omega}_p^2(\mathbf{r})$ and $\tilde{\omega}_p^2(\mathbf{k})$ stand, respectively, for the function defined as the square of the local plasmon frequency at \mathbf{r} and its Fourier transform, whereas ω_p is just the value of this parameter in the homogeneous medium. Out of simplicity the induced charge density will be referred as $\rho(\mathbf{k}, \omega)$ and $\hat{\rho}(Q, \omega)$ for its projection in the parallel direction (k_x, k_y) using the notation $\rho_0(\mathbf{k}, \omega)$ for the probe charge density. The convention for the Fourier transform used in this paper is as follows:

$$f(\mathbf{r}, t) = \frac{1}{(2\pi)^4} \int_{-\infty}^{\infty} d\mathbf{k} \int_{-\infty}^{\infty} d\omega e^{i(\mathbf{k}\cdot\mathbf{r} - \omega t)} f(\mathbf{k}, \omega). \quad (3)$$

II. DIELECTRIC APPROACHES

Figure 1(a) shows the impact parameter dependence of the transverse force $F_x(b)$ experienced by a 100-keV electron in different dielectric approaches, a magnitude directly related to the TMT, $\Delta p_x / \Delta z = v^{-1} F_x$.

The plot LDT corresponding to an abrupt Drude interface, calculated after Ref. [9], clearly reflects some of the inconsistencies of this approach; given that the induced charge is confined on the surface, actually the target excitations do not carry transverse momentum at all. The so-calculated transverse force is the consequence of the interaction of the probe with the charge induced on the surface, the so-called *electron*

wake, which because of the causality of the response function, appears behind the probe as shown schematically in the inset of Fig. 1(a) [30]. This force has, besides the longitudinal component responsible for the stopping power, a projection into the normal direction which is not associated with excitations carrying transverse momentum. A surprising result of this plot is the finite value of the force in the limit $b \rightarrow 0$ in contrast with the divergent limit of the force associated with longitudinal excitations. In this limit the surface density gets divergent, but in the transverse force, this divergence is compensated by the vanishing projection of the force into the normal direction so that F_x remains finite and attractive (negative). The finiteness of this limit is a general result, valid for any causal dielectric function [31,32]; in the particular case of a Drude $\epsilon(\omega)$ it verifies $\lim_{b \rightarrow 0} F_x = -(\omega_s/v)^2$, where ω_s is the surface plasmon frequency [33]. The lack of robustness of this limit is revealed by the fact that the transverse force becomes divergent in the retarded theory even at moderate relativistic velocities [31]. This is an inherent shortcoming of the LDT where electrons in the metal are subjected to a holonomic constraint, $\hat{\rho}(x, Q, \omega) \sim \delta(x)$ so that the force associated with this restriction should be taken with some caution. We conclude that the force calculated in LDT is likely to be correct for distant collisions where the normal component of the force exerted by the probe on the surface density is negligible compared with the force constraining it into the surface, but it does not hold for grazing incidence where the exciting force is large enough to overcome this constraint.

The LDT has been used to study the momentum transfer to nanoparticles in the framework of the retarded theory where radiation opens a new inelastic channel [5,15–18]. In these works the crossover between attractive and repulsive values of the transverse force as the impact parameter gets smaller, reported by Batson and co-workers [12], is qualitatively reproduced. Nevertheless, a recent revision of the problem by Castrejón-Figueroa and co-workers has concluded that the force remains always attractive, considering that the crossover found in previous works was due to the use of noncausal experimental dielectric functions as well to deficiencies in the computation [19]. Regardless of whether there is such a crossover, the limitations of the local approach at small impact parameter seriously question the soundness of these results. A simple way of introducing quantal effects into the medium response is through the use of a nonlocal dielectric function, $\epsilon(\mathbf{k}, \omega)$, an approach which relaxes the constraint to the surface of the induce charge. Nevertheless, this approach also turns out to be troublesome. On one hand, a function which depends just on \mathbf{k} implies translational invariance of the response in real space and, therefore, cannot cope with the effects derived from the strong anisotropy in the direction normal to the surface. On the other hand the use of boundary conditions reduces the applicability of this approach to abrupt interfaces so that effects derived from the electron density spill out are not considered. Besides, the more usual procedure, i.e., the so-called *specular reflection model* (SRM) [34,35], averages the response in the direction normal to the surface. Following Ref. [36], the potential $\phi_{\text{ind}}(\mathbf{r})$ is induced by an external probe. ($b > 0$), in the right half space ($x > 0$) can be written in terms of excitations of energy $\hbar\omega$ and parallel

momentum component ($k_y, \omega v^{-1}$) as

$$\phi_{\text{ind}}(\mathbf{r}, t) = \frac{1}{2\pi v} \int d\omega \int dk_y \left[\frac{\tilde{\epsilon}(Q, \omega) - 1}{\tilde{\epsilon}(Q, \omega) + 1} \right] \frac{e^{-Q(x+b)}}{Q} \times e^{ik_y y} e^{i(\omega/v)(z-vt)}, \quad (4)$$

where $Q = \sqrt{k_y^2 + \frac{\omega^2}{v^2}}$ and the function $\tilde{\epsilon}(Q, \omega)$ is defined as

$$\tilde{\epsilon}(Q, \omega) = \frac{\pi}{Q} \left[\int \frac{dk_x}{(k_x^2 + Q^2)\epsilon(\mathbf{k}, \omega)} \right]^{-1}. \quad (5)$$

The function $\tilde{\epsilon}(Q, \omega)$ is a k_x -averaged surface response, insensitive to the dependence on this component of the exciting field. We have also added the plot calculated in the Local Approach for a Dielectric Interface (LADI), where the response is characterized by a local dielectric function $\epsilon(x, \omega)$ (see Appendix A). This approach should be considered just as a semilocal one, in the sense that local effects only depend on the parallel momentum. Figure 1(a) also plots the force $F_x(b)$ calculated from Eq. (4) with two different nonlocal dielectric functions. The one labeled as SRM PPA corresponds to the *plasmon pole approximation* [37],

$$\epsilon(k, \omega) = 1 - \frac{\omega_p^2}{\omega(\omega + i\gamma) - \beta^2 k^2 - \frac{1}{4}k^4}, \quad (6)$$

where the βk^2 and k^4 terms account for hydrodynamic pressure and single electron excitations, respectively. The plot SRM HF corresponds to the so-called *hydrodynamic function*, which is defined, such as Eq. (6) without the k^4 term in the denominator [38]. The plots corresponding to these approaches are almost identical to that of the LDT, even in the limit $b \rightarrow 0$, revealing that in these models the TMT also derives from the interaction of the probe with the surface wake without the contribution from the displacement of the induced density in the normal direction. This fact is a physical consequence of the reflection of the induced density on the surface implicit in the SRM where the transverse momentum carried by the incoming and outgoing electrons exactly balance one another.

We have also added the plot of the force induced by the diffuse interface shown in Fig. 1(b), characterized by a local dielectric function $\epsilon(x, \omega)$ (see Appendix A). For large impact parameters this plot does not differ significantly from the ones corresponding to sharp interfaces. Here the large wavelength components of the exciting field are unable to probe the spatial extension of the interfacial layer so that the induced field is insensitive to the thickness of the interface. Below the value of $b \sim \lambda$ the force grows very fast, getting divergent for beam trajectories inside the interface. Note that in this calculation the contribution of the screened bulk density of the probe $\rho_0(b, \omega)/\epsilon(b, \omega)$ to the total potential has been removed so that that the force is just due to the interaction with the finite contribution of the interface to the induce potential. The divergent behavior of this plot as $b \rightarrow 0$ confirms the unsoundness of the dielectric formalism to calculate the TMT at grazing incidence.

III. LOCAL DENSITY HYDRODYNAMIC APPROACH (LDHA)

The interaction of a fast electron with a metallic interface is now tackled in the Local Density Hydrodynamic Model where the target is assumed to be a metal, described by the *local* parameters of an electron gas corresponding to an unperturbed local electron density $n(x)$, which is assumed to vary smoothly in the direction normal to the interface. For a free electron target, the two *local* parameters $\tilde{\omega}_p(x)$ and $\tilde{\beta}^2(x)$ of the dielectric response can be written as

$$\tilde{\omega}_p^2(x) = 4\pi n(x), \quad \tilde{\beta}^2(x) = \frac{3}{5}[3\pi^2 n(x)]^{2/3}. \quad (7)$$

Following Ref. [21], the induced charge density $\rho(\mathbf{k}, \omega)$ is given by the solution of a *Fredholm integral equation of the second kind*,

$$\begin{aligned} \left[\omega(\omega + i\gamma) - \frac{1}{4}k^4 \right] \rho(\mathbf{k}, \omega) - \frac{1}{2\pi} \int dq_x \frac{\mathbf{q} \cdot \mathbf{k}}{q^2} [\tilde{\omega}_p^2(k_x - q_x) \\ + \tilde{\beta}^2(k_x - q_x)q^2] \rho(\mathbf{q}, \omega) = \frac{1}{2\pi} \int dq_x \frac{\mathbf{q} \cdot \mathbf{k}}{q^2} \tilde{\omega}_p^2(k_x - q_x) \\ \times \rho_0(\mathbf{q}, \omega), \end{aligned} \quad (8)$$

where $\rho_0(\mathbf{k}, \omega)$ stands for the probe charge density and $\tilde{\omega}_p^2(k_x)$ and $\tilde{\beta}^2(k_x)$ are the Fourier transforms of the corresponding functions in the real space. In the left-hand term of Eq. (8) the boundary independent term $\frac{1}{4}k^4$ has been added so that in the limit of a homogeneous medium $\tilde{\omega}_p(x) = \omega_p$, the corresponding induced density calculated with the PPA [Eq. (6)] is recovered,

$$\rho(\mathbf{k}, \omega) = \frac{\omega_p^2}{\omega(\omega + i\gamma) - \omega_p^2 - \beta^2 k^2 - \frac{1}{4}k^4} \rho_0(\mathbf{k}, \omega). \quad (9)$$

Equation (8) can be formally written in terms of a couple of linear operators \mathcal{L} and \mathcal{R} as

$$\rho(k_x, Q, \omega) = \mathcal{L}^{-1} \mathcal{R} \rho_0(q_x, Q, \omega), \quad (10)$$

where

$$\begin{aligned} \mathcal{L}(k_x, q_x) &= \left[\omega(\omega + i\gamma) - \frac{1}{4}k^4 \right] \delta(k_x - q_x) \\ &\quad - \frac{1}{2\pi} \frac{\mathbf{q} \cdot \mathbf{k}}{q^2} [\tilde{\omega}_p^2(k_x - q_x) + \tilde{\beta}^2(k_x - q_x)q^2] \\ \mathcal{R}(k_x, q_x) &= \frac{1}{2\pi} \frac{\mathbf{q} \cdot \mathbf{k}}{q^2} \tilde{\omega}_p^2(k_x - q_x), \end{aligned} \quad (11)$$

and where $[\mathcal{L}f](k_x) \equiv \int dq_x \mathcal{L}(k_x, q_x) f(q_x)$. Equation (10) states the linearity of the response, in terms of a unique linear operator $\mathcal{L}^{-1} \mathcal{R}$, which contains all the information about the excitations of the medium, and which plays the same role as the reciprocal dielectric function $\epsilon(\mathbf{k}, \omega)^{-1}$ in the dielectric theory for a nonbounded medium. The fact that one can write the medium polarization by means of a single response function for all the probe trajectories is a theoretical advantage over the dielectric approaches where the solution depends on whether the probe travels inside or outside the medium.

The linearity of the response stated by Eq. (8) implies the validity of the convolution approach to the interaction of extended probes stated by Ritchie and Howie [39]. This

convolution is valid as far one can neglect the dispersion of the beam due to the interaction with the interface. This condition can be understood as the classical counterpart of the *neglecting the probe recoil* proviso in the quantal approach of Ref. [39]. Although in the case of large interfaces the dispersion of the beam can be relevant, in the case of small targets this assumption is arguably fine.

It is interesting to compare Eq. (8) with the general expression derived from the constitutive relation (CR), which states the linearity between the polarizability \mathbf{P} and the total electric-field \mathbf{E} through the nonlocal susceptibility χ . From the standard CR, the linearity of the response can be recast in terms of both the induced and the free charge densities as

$$\begin{aligned} \rho(\mathbf{k}, \omega) + \frac{1}{2\pi^2} \int \frac{\mathbf{k} \cdot \mathbf{q}}{q^2} \chi(\mathbf{k}, -\mathbf{q}, \omega) \rho(\mathbf{q}, \omega) d\mathbf{q} \\ = -\frac{1}{2\pi^2} \int \frac{\mathbf{k} \cdot \mathbf{q}}{q^2} \chi(\mathbf{k}, -\mathbf{q}, \omega) \rho_0(\mathbf{q}, \omega) d\mathbf{q} \end{aligned} \quad (12)$$

(see Appendix B). Equation (12) is also a *Fredholm equation*, formally similar to Eq. (8). The difference between both approaches lies on the fact that in Eq. (12) both densities that of the probe ρ_0 and the induced one ρ appear on an equal footing, whereas in Eq. (8), the pressure term is missing in the right hand term (RHT). This is because in the hydrodynamic approach the force corresponding to the pressure correction has been considered as an internal force of the electron gas, and, consequently, it is not applied to the field created by the probe.

The inverse Fourier transform of Eq. (8) allows recasting it in the real space in an invariant form (independent of the coordinate system) as

$$\begin{aligned} \frac{1}{4} \nabla^2 \nabla^2 \rho(\mathbf{r}, \omega) + \tilde{\beta}^2(\mathbf{r}) \nabla^2 \rho(\mathbf{r}, \omega) + [(\omega + i\gamma)\omega - \tilde{\omega}_p^2(\mathbf{r})] \\ \times \rho(\mathbf{r}, \omega) + \frac{1}{4\pi} \nabla \tilde{\omega}_p^2 \nabla \int d\mathbf{r}' \frac{\rho(\mathbf{r}', \omega)}{|\mathbf{r}' - \mathbf{r}|} + \nabla \tilde{\beta}^2 \nabla \rho(\mathbf{r}, \omega) \\ = \tilde{\omega}_p^2(\mathbf{r}) \rho_0(\mathbf{r}, \omega) - \frac{1}{4\pi} \nabla \tilde{\omega}_p^2 \nabla \int d\mathbf{r}' \frac{\rho_0(\mathbf{r}', \omega)}{|\mathbf{r}' - \mathbf{r}|}, \end{aligned} \quad (13)$$

which can be applied with targets of nonplanar geometries. In the case of targets with simple geometries (spheres, cylinders, films, and so on) Eq. (13) turns out to be separable so that the problem is reduced to a set of ordinary integrodifferential equations.

Equation (8) [and arguably Eq. (13)] is an extension of the Poisson equation $\nabla[\epsilon(\mathbf{r}, \omega) \nabla \phi(\mathbf{r}, \omega)] = 4\pi \rho_0(\mathbf{r}, \omega)$ for a free electron gas with a position-dependent Drude dielectric function,

$$\epsilon(x, \omega) = 1 - \frac{\tilde{\omega}_p^2(x)}{\omega(\omega + i\gamma)}, \quad (14)$$

where quantal corrections have been incorporated so that the resulting equation presents the correct limits:

(a) In the case of a local response $\tilde{\beta}^2(x) \equiv 0$, and removing the term k^4 in Eq. (8) [or the corresponding $\nabla^2 \nabla^2 \rho(\mathbf{r}, \omega)$ term in Eq. (13)], these expressions reduce to the Poisson equation with the dielectric function given by Eq. (14). In particular, for sharp interfaces, $\tilde{\omega}_p(x) = \omega_p H(-x)$, where $H(x)$ is the Heaviside function, the solution can be recast in terms

of a surface density, leading to an expression fully equivalent to that of the *boundary element method* [4].

(b) In the case of sharp interfaces the results of the SRM with the HF are recovered as an approximated solution of Eq. (8) for beam trajectories both inside and outside the medium [21]. Agreement with the SRM has also been found in films [40] and spheres [41]. Note that the present model assumes the differentiability of both $\tilde{\omega}_p(x)$ and $\tilde{\beta}^2(x)$, and, consequently, that of the induced density so that in the case of an abrupt interface only an approximated solution Eq. (17) can be found. Introducing the k^4 term in Eq. (17) should require the continuity of higher derivatives of the electron-gas parameters, and, consequently, the sharp interface model would be still more inconsistent.

Following Ref. [21] now we apply this model to the case of a diffuse Al interface where the *local* charge-density $n(x)$ is modeled by a fit of the profile calculated by Lang and Kohn [20] [see Fig. 1(b)],

$$n(x) = \frac{n_0}{2} \left[1 - \operatorname{erf}\left(\frac{x}{\lambda}\right) \right], \quad (15)$$

where n_0 is the bulk density of the electron gas and erf stands for the error function [42]. Lang's tabulated data for Al ($r_s = 2.12a_0$, or $\hbar\omega_p = 15.3$ eV) are reasonably well fitted with $\lambda = 1.56a_0$. The corresponding *local* plasmon frequency is as follows:

$$\begin{aligned} \tilde{\omega}_p^2(x) &= \frac{\omega_p^2}{2} \left[1 - \operatorname{erf}\left(\frac{x}{\lambda}\right) \right] \rightarrow \tilde{\omega}_p^2(k_x) \\ &= \omega_p^2 \left[\pi \delta(k_x) + \frac{i}{k_x} e^{-(1/4)\lambda^2 k_x^2} \right], \end{aligned} \quad (16)$$

and the corresponding bulk value of parameter β^2 is then $\beta^2 = 0.49$ a.u. Out of simplicity the same spatial dependence has been considered for $\tilde{\beta}^2(x)$.

For probes moving parallel to the interface where the density can be factorized as $\rho(\mathbf{k}, \omega) = \hat{\rho}(k_x, Q, \omega) \delta(\omega - k_z v)$, Eq. (8) writes

$$\begin{aligned} &\left[\omega(\omega + i\gamma) - \frac{1}{2}(\omega_p^2 + \beta^2 k^2) - \frac{1}{4}k^4 \right] \hat{\rho}(k_x, Q, \omega) + \frac{i}{2\pi} \mathbb{P} \\ &\times \int dq_x \frac{\mathbf{k} \cdot \mathbf{q}}{q^2} [\omega_p^2 + \beta^2 q^2] \frac{e^{-(\lambda^2/4)(q_x - k_x)^2}}{q_x - k_x} \\ &\times \hat{\rho}(q_x, Q, \omega) = 2\pi \tilde{\omega}_p^2(b) e^{-ik_x b} \\ &+ i\omega_p^2 \int dq_x \frac{q_x e^{-iq_x b}}{q^2} e^{-(\lambda^2/4)(q_x - k_x)^2}, \end{aligned} \quad (17)$$

where \mathbb{P} stands for the Cauchy principal value of the integral.

In the Appendix of Ref. [21] the computational method used to solve Eq. (17) is discussed. It is worth noting that the addition of the k^4 term in the left hand term (RHT) of this equation works as an effective cutoff reducing the range of k_x contributing to the medium response, and, consequently, the necessity of extending the limits of the integral on q_x beyond the physically meaningful limits in order to get a good convergence of the result. This reduction significantly improves both the accuracy and the computational requirements of the calculation.

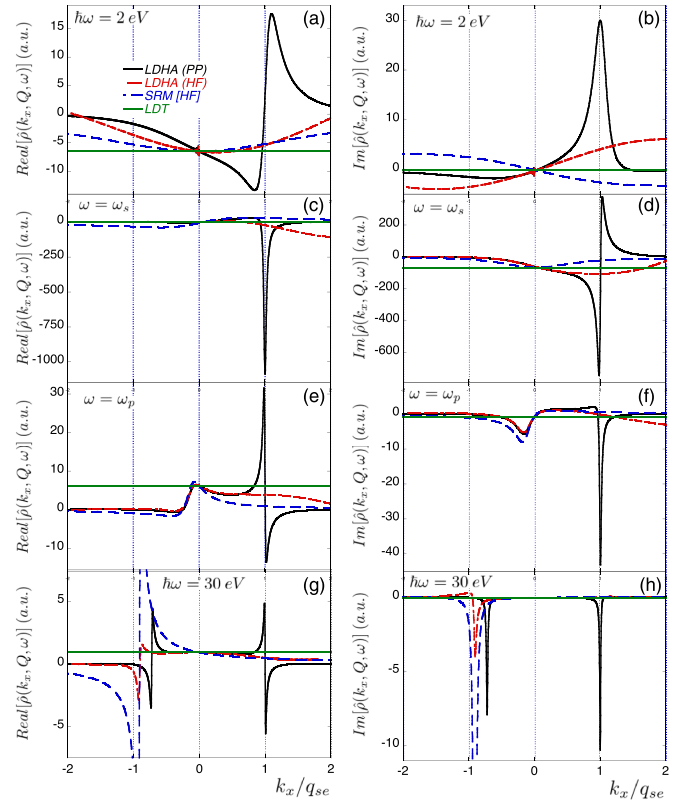


FIG. 2. k_x dependence of the real and imaginary parts of the charge-density $\hat{\rho}(k_x, Q, \omega)$ induced by a 100-keV electron moving with impact parameter $b = 0.1$ nm near an Al diffuse surface ($\lambda = 1.56a_0$) for four different values of ω ; $\hbar\omega = 2$ eV [plots (a) and (b)], $\omega = \omega_s$ [(c) and (d)], $\omega = \omega_p$ [(e) and (f)], and $\hbar\omega = 30$ eV [(g) and (h)]. In all the cases of $k_y = 0$. The normalization factor $q_{se} = \sqrt{2\omega - Q^2}$ corresponds to the threshold of single electron excitations. Labeling as stated in the beginning of Sec. IV. Values of the Al dielectric parameters as in Fig. 1.

IV. RESULTS

In this section we analyze the results of this model for a 100-keV electron ($v = 76$ a.u.) passing near or through an Al interface characterized as stated in the previous section. Plots of the current theory are labeled as the local density hydrodynamic approach (LDHA) [or LDHA (HF) for results obtained after removing from Eq. (17) the k^4 term]. Results corresponding to the different dielectric approaches are labeled as in Fig. 1.

A. The induced charge density

Figure 2 shows the k_x dependence of the induced charge-density $\hat{\rho}(k_x, Q, \omega)$ for four different values of the excitation energy for an electron passing at grazing incidence ($b = 0.1$ nm). In all the cases $k_y = 0$. In addition to the LDHA solutions, we have also added plots corresponding to the analytic solution corresponding to a sharp interface in the nonlocal dielectric formalism [SRM (HF)] as calculated in Ref. [21],

$$\hat{\rho}(k_x, Q, \omega) = \frac{2\pi i \omega_p^2 (Q + \mu)}{\omega_p^2 - 2\beta^2 \mu (Q + \mu)} \frac{e^{-Qb}}{k_x + i\mu}, \quad (18)$$

where $\mu = Q^2 + \beta^{-2}[\omega_p^2 - \omega(\omega + i\gamma)]^{1/2}$ [21] and in the LDT, which is the limit $\beta \rightarrow 0$ of the previous expression,

$$\hat{\rho}(k_x, Q, \omega) = \frac{2\pi\omega_p^2}{\omega_p^2 - 2\omega(\omega + i\gamma)} e^{-Qb}. \quad (19)$$

At all the frequencies, differences among the plots are hardly noticeable at small values of k_x . It implies that the (Q, ω) component of the total induced charge along the interface $\int dx \tilde{\rho}(x, Q, \omega) = \tilde{\rho}(k_x = 0, Q, \omega)$ is the same in all the models, a fact that reflects the fact that all them require the same induced charge to screen the external field. A further consequence is the value of the total induced charge, which in the LDHA can be calculated as

$$q_{\text{tot}} = \frac{1}{2\pi} \lim_{\omega \rightarrow 0} \tilde{\rho}\left(k_x = 0, Q = \frac{\omega}{v}, \omega\right), \quad (20)$$

and which numerically is found to be $q_{\text{tot}} = -1$, the same value obtained in both dielectric approaches.

As expected, the most relevant differences appear for large k_x where the LDH features two well-defined resonances. The largest one occurs at $k_x = q_{se} \equiv [2\omega - Q^2]^{1/2}$, a value which corresponds to the excitation of a free electron with energy ω . This resonance is present at all the frequencies, but its intensity is maximum at the surface-plasmon frequency ω_s , showing a fast decay above and below this value.

The other resonance in the LDHA plots only appears for frequencies above ω_p [plots (g) and (h)] and it exactly corresponds to the negative value of the pole of Eq. (9), describing the decay of a bulk plasmon into an electron-hole pair.

Also above ω_p the plots corresponding to the *hydrodynamic approach* LDHA (HD) and SRM (HF) feature a broad resonance near $k_x \sim -q_{eh}$. This is a coincidental agreement; actually these structures correspond to the pole of $\epsilon(k, \omega)^{-1}$ in the HF, i.e., at $k_x = [(\omega^2 - \omega_p^2)/\beta^2]^{1/2}$ (in the limit $Q \rightarrow 0$). In these plots the resonance appears at $k_x = -1.3a_0^{-1}$, a value well outside the validity range of the HF; therefore, these resonances are unphysical artifacts of these dielectric approaches with no real physical meaning.

For $k_y = 0$ the function $\hat{\rho}(k_x, Q, \omega)$ presents a weak dependence on the impact parameter. Actually plots corresponding to grazing ($b = 0.1$ nm) and aloof ($b = 1$ nm) incidence are hardly distinguishable, a result also found in the dielectric approaches [Eqs. (18) and (19)]. This is a consequence of the smallness of Q in the limit $k_y = 0$, ($Q \sim 5 \cdot 10^{-3} a_0^{-1}$ around ω_s); in this domain of the (k_x, ω) space the normal component of the exciting field on the interface goes as $\sim e^{-Qb}$, so it depends weakly on b and, therefore, so does the polarization of the target. Contributions of higher k_y or larger impact parameters change significantly the induced density. Therefore, the plots of the Fig. 2 provide a good picture of the response function of the interface at large parallel wavelengths, playing a role analogous to that of the surface function $[\epsilon(\omega) - 1]/[\epsilon(\omega) + 1]$ in the LDT.

Normal modes of the interface do not correspond to a single k_x value. Nevertheless, in the next subsections we have split the k_x contribution to the momentum transfer [Eqs. (1) and (2)] in two domains; that of small k_x values [$|k_x| < \frac{1}{2}q_{se}$, labeled CE, loosely represents the momentum carried by collective oscillation of the electron gas. The remaining domain

($|k_x| > \frac{1}{2}q_{se}$), labeled SE, basically contains the contribution of single electron excitations with a much weaker contribution from the decay of bulk plasmons into electron-hole pairs for energies above $\hbar\omega_p$. The limit $\frac{1}{2}q_{se}$ in this analysis is rather arbitrary, but the plots of Fig. 2 indicate that both contributions should not critically depend on the exact value of this limit so that this splitting helps to understand the role of the different range of k_x to the probe scattering.

B. Longitudinal momentum transfer: energy-loss spectra

In the customary adiabatic approximation the total energy loss per unit length can be written as

$$\frac{\Delta E}{\Delta z} = v \frac{\Delta p_z}{\Delta z} = \int_0^\infty \frac{d\mathcal{P}(\omega)}{dz d\omega} \omega d\omega, \quad (21)$$

where $\frac{d\mathcal{P}(\omega)}{dz d\omega}$, the energy-loss probability per unit length, can be derived from Eq. (1),

$$\frac{d\mathcal{P}(\omega)}{dz d\omega} = \frac{1}{\pi^3 v^2} \int_0^\infty dk_y \int_{-\infty}^\infty \frac{dk_x}{k^2} \text{Im}[\tilde{\rho}(k_x, Q, \omega) e^{ik_x b}]. \quad (22)$$

Figure 3 shows the EELS for four different values of the impact parameter b . In addition to the total loss probability [labeled as LDHA (total)] we have also plotted (scaled by a factor of 10) the contribution of the high values to the k_x integral in Eq. (22) [labeled LDHA (SE)]. In all the cases SE contribution around the surface loss peak probes to be almost two orders of magnitude smaller than that of the collective excitations, a result which confirms the statement that collective excitations provide the main contribution to the energy loss. The fact that at some impact parameter this correction turns out to be negative [plots (b) and (c)] should not be interpreted as *accelerating* excitations; as pointed out before, k_x is not a proper label for the interface modes, and only the total value of the integral (22) has a sound physical meaning. Actually such negative contributions are also found in the dielectric models for some values of k_x when one calculates the loss probability [Eq. (22)] with the induced charge density calculated in the dielectric approaches [Eqs. (18) and (19)].

In Fig. 3 spectra calculated with different dielectric approaches have been added to allow comparison. For external trajectories the plots corresponding to LDHA and to LADI are almost identical, showing that the dispersion associated to the smoothness of the density profile turns out to be the more relevant source of nonlocal corrections and that quantal corrections in Eq. (17) do not lead to appreciable differences in the loss spectra. Corrections relative to the SRM spectra are twofold; on one hand, LDHA broadens and reduces the intensity of the peak, and on the other hand the losses are centered at the surface-plasmon frequency ω_s without the blueshift featured by the PPA plots. The LDHA plots are very similar to their counterparts in Ref. [21].

For penetrating probes, both the current theory and the SRM lead to rather similar results. These plots exhibit the so-called *Begrenzung effect* [2]: at the small impact parameter [Fig. 3(c)] the spectra basically consist of a single peak a little above ω_s , remaining excitation of bulk plasmons almost totally inhibited, whereas for trajectories away from the interface [Fig. 3(d)] the intensity of the bulk peak grows at the expense of the surface one. In Figs. 3(c) and 3(b) the surface

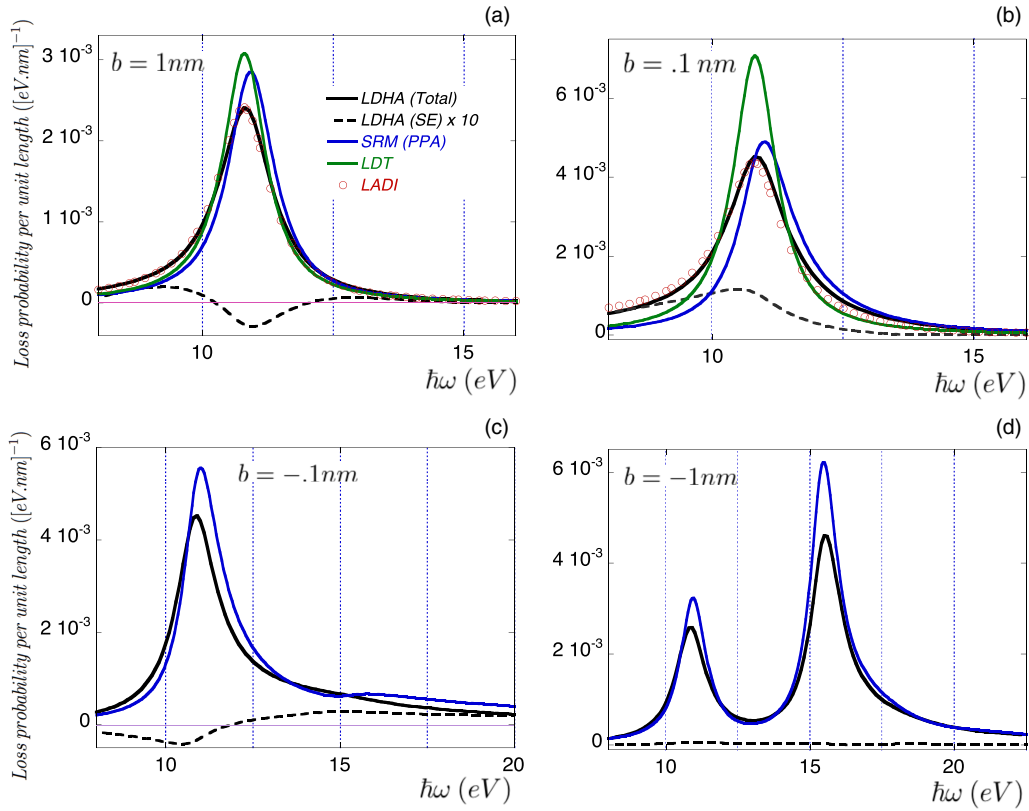


FIG. 3. Energy-loss spectra for an 100-keV electron traveling parallel to an Al interface for four different impact parameters: (a) $b = 1$ nm, (b) $b = 0.1$ nm, (c) $b = -0.1$ nm, and $b = -1$ nm (d). Continuous and broken black plots correspond to the total loss probability and the contribution of single e^- excitations, respectively. Results corresponding to different dielectric approaches are labeled as stated in the beginning of Sec. IV. In all the cases LDA (SE) plots have been scaled up by a factor of 10 to improve their visibility.

peak in the LDHA presents a weak blueshift relative to ω_s ($\Delta\omega \sim 0.05$ eV), which is smaller than that of the PPA plots ($\Delta\omega \sim 0.1$ eV), whereas the blueshift of the bulk peak in Fig. 3(d) is the same in both approaches. A possible explanation for the difference in the shift of the surface peak is that interface excitations in the LDHA occur in a spatial region thicker than the one corresponding to the PPA so that it could be expected for a weaker pressure correction in the response.

C. Transverse momentum transfer

The transverse component of the force acting on the probe $F_x = v \frac{\Delta p_x}{\Delta z}$ can be calculated from Eq. (2) as an integral over ω ,

$$F_x = \int_0^\infty \mathcal{F}(\omega) d\omega, \quad (23)$$

where the spectral function $\mathcal{F}(\omega)$ contains the contribution of all the wave vectors to an excitation of frequency ω ,

$$\mathcal{F}(\omega) = \frac{1}{\pi^3 v} \int_0^\infty dk_y \int_{-\infty}^\infty dk_x \frac{k_x}{k^2} \text{Im}[\tilde{\rho}(k_x, Q, \omega) e^{ik_x b}]. \quad (24)$$

Figure 4 shows the impact parameter dependence of this component for a 100-keV probe, as well the contribution of both collective (CE) and SE excitations. As expected, for distant trajectories $b > 1$ nm where the contribution of large k_x values (red line) is negligible, the LDHA leads to the same

results as the LDT, a further consequence of the similarity of the interface response around $k_x = 0$ seen in Sec. III. The likeness of these plots confirms that at aloof incidence the origin of the force is basically the interaction with the wake induced behind the probe.

At the grazing incidence, although, collective excitations induce a positive (repulsive) force on the probe, which corresponds to a negative momentum transfer to the electron gas, i.e., to a displacement of the valence electrons towards the bulk. This large momentum transfer is almost exactly compensated by the negative contribution of large k_x values so that the total force at the interface turns out to be almost two orders of magnitude smaller than the partial contributions. This balance also occurs for trajectories inside the medium ($b < 0$). Given that the attractive contribution of high- k_x values mainly arises from single electron excitations, momentum conservation implies that the so-excited electrons carry positive momentum, i.e., they move outwards from the interface. The balance between collective and single electron contributions shown in Fig. 4(b) indicates that at grazing incidence most of the transverse momentum carried by collective excitations is transferred to a single electron, which is emitted as a *secondary electron*. The impact parameter dependence of the momentum carried by these excitations shown in this plot presents a reasonable qualitative agreement with experimental data on secondary electron emission (SEE) reported by Howie and Milne [43]. Finer information about these excitations

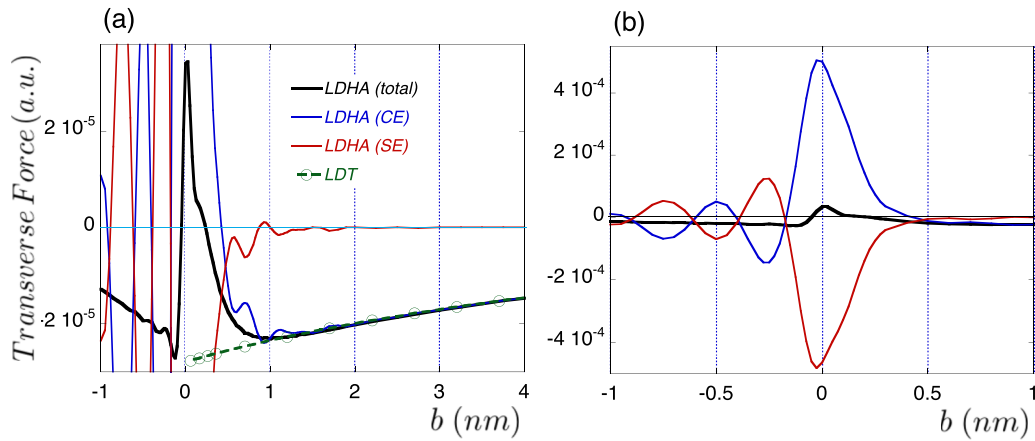


FIG. 4. (a) Transverse force experienced by a 100-keV electron moving parallel to an Al interface as a function of the impact parameter b (black line). Contributions of both collective (blue line) and single electron (red line) excitations have also been plotted. The plot corresponding to LDT has been added to allow comparison. (b) Details of the LDHA plots.

would be provided by the current density $\mathbf{J}(\mathbf{k}, \omega)$, a magnitude used in the derivation of Eq. (8) [21], but the fact that $\mathbf{J}(\mathbf{r})$ is not irrotational in the interface implies that the knowledge of the induced density is not sufficient to solve the continuity equation $\nabla \cdot \mathbf{J} = i\omega\rho$.

The TMT to the target is then the one carried by the collective excitations [i.e., the opposite of the blue line in Fig. 4(b)]. The momentum of the target then features the impact parameter dependence experimentally found: The force experienced by the target is attractive (positive) for distant collisions, turning to repulsive at grazing incidence [12]. The SEE was suggested by Howie as the possible mechanism responsible of the repulsive force [44].

Below $b = 1$ nm, both collective and single electron contributions present small correlated oscillations, which could correspond to the excitations of the so-called *multipolar surface plasmons* [45,46].

In Fig. 5(a) we plot the spectral function $\mathcal{F}(\omega)$ for a probe at grazing incidence. Around ω_s the plot corresponding to collective excitations and to the SRM are rather similar, reflecting the ability (inability) of the electron gas to answer in phase to the exciting field below (above) ω_s . The negative contribution of single electron excitations is also peaked at ω_s , turning negligible above ω_p . Below $\omega = 4$ eV the total

contribution turns to be positive. In this frequency range the resonance associated with single e^- excitations is very broad [Figs. 2(a) and 2(b)], and, consequently, the splitting between both collective and single e^- excitations becomes rather imprecise. These plots imply that in this frequency range the induced charge is pushed into the bulk so that the screening of the surface cations of the crystal is weakened in the phonon range, a fact that suggests the need to take into account the crystal structure beyond the uniform background approach. The weakening of the screening of the metallic cations in this frequency range could explain the strong perturbation of the surface experimentally observed.

In Fig. 5(b) we represent the integral of the spectral function as a function of the integration limit ω . The slow convergence of the plot corresponding to collective excitations, and, consequently, that of the total TMT, supposes that the Drude-like response of the electron gas has been extended well outside its actual range of applicability so that the total value of these magnitudes is not physically meaningful. In particular, this observation calls the sign crossover of the total force into question. Nevertheless, the contribution coming from secondary electron excitation is restricted to the valence electron region so that the recoil of the target at close trajectories is a sound and robust result.

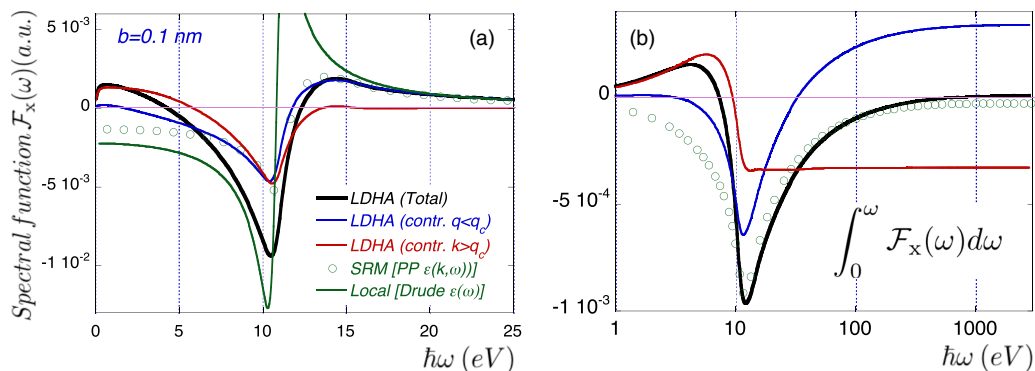


FIG. 5. (a) Spectral function $\mathcal{F}(\omega)$ for 100-keV electrons at grazing incidence ($b = 0.1$ nm) in different approaches. (b) Integral of $\mathcal{F}(\omega)$ as a function of the upper- ω integration limit.

The balance between the momentum carried by collective and single electron contributions explains the fact that at grazing incidence the averaged deflection of the probe is much smaller than the one corresponding to the recoil of the target, so that most of the electrons of the probe are collected inside a small deflection angle $\Delta\theta$; for a probe traveling by a surface of length ΔL , $\Delta\theta = F_x \Delta L v^{-2}$, which at grazing incidence for a 100-nm-long target leads to a small deflection $\Delta\theta \sim 10^{-2}$ mrad, a value of the same order than that calculated in the dielectric theory [10,11]. Nevertheless, the dispersion of the scattered electrons from this average value can be estimated from Eq. (2). According to Fig. 5(a) the contribution of single electron excitations reaches up to ω_p so that for not excessively long paths where multiple scattering can be neglected, the largest deflection would correspond to $\Delta\theta = q_{se}(\omega_p)v^{-1} \sim 14$ mrad, a value in accordance with the one used in STEM setups.

V. CONCLUSIONS

We have studied nonlocal effects in the scattering of fast probes by a metallic target, considering both quantal corrections as well those derived from the spatial profile of the charge density on the interface. First, we have analyzed the shortcomings of the dielectric approaches to deal with the response of the target to large wave vectors, and then we have introduced a hydrodynamic approach (LDHA) which tackles both sources of nonlocal effects, keeping quantal corrections to the same level as the *lasmon pole approach* in the dielectric theory.

An extension of this theory to deal with samples of arbitrary geometry is also presented.

For nonpenetrating beams, nonlocal effects in EELS prove to be basically ruled by the spatial smoothness of the interface with negligible contribution of large momentum excitations both at grazing and aloof incidence. On the other hand, nonlocal corrections to the momentum transfer in the normal direction present a strong dependence on the impact parameter; these corrections are negligible in aloof trajectories, but they are strong enough to change the sign of the momentum transfer at grazing incidence.

In the case of large interfaces where there is no radiation, three-momentum carriers are involved in the scattering process; the probe, the target, and the emitted secondary electrons. LDHA allows identify the contribution of collective and single electron excitations, showing that at grazing incidence the emission of secondary electrons turns out to be the most efficient channel for the decay of surface plasmons. Secondary electron emission is, therefore, a surface effect, significant just at small impact parameters, and the recoil associated with it probes to be responsible of the repulsive force experienced by the target. Although, in large targets this recoil is too small to lead to observable displacement of the target, in the case of nanoparticles where the ratio surface/bulk is much larger, this recoil could be measurable, as experimentally found by Batson and collaborators [17]. In this last case, one should also take into account the momentum carried by the radiation, but given that its leading contribution is dipolar, its corrections to the TMT is likely to be negligible.

As pointed out in Ref. [21], the applicability of the LDHA as presented in this paper is limited to free-electron interfaces. In the same reference, a way to extend the model to deal with transition metals was suggested by modeling the valence electrons of the target as a set of n electron bands, each of them characterized by a pair of local parameters: $\tilde{\omega}_p^2$ and $\tilde{\beta}^2$ (where the index k labels the electron band), plus the frequency Ω_k of a binding oscillator. The bulk values of these parameters could be obtained by from the parametrization of the corresponding bulk dielectric function (see, for instance, Ref. [47]). Then Eq. (8) should be split into a set of k integrodifferential equations, coupled by the interaction between the induced charge density of all bands in the integral of the LHT of this equation. Although the complexity of this system increases with the number of bands, the presence of the correction in k^4 in the LHT of Eq. (8) assures a significant reduction of the k_x interval needed to get good convergence, and, therefore, it can make this calculation affordable.

ACKNOWLEDGMENTS

I wish to thank Professor A. Howie, Professor R. Barrera, and Professor N. Zabala for many stimulating discussion and suggestions. Part of this paper was carried out at during my stay at the Departamento de Polímeros y Materiales Avanzados: Física, Química y Tecnología, Facultad de Químicas, UPV/EHU, and Materials Physics Center (CSIC-UPV/EHU), MPC in San Sebastian (Spain).

APPENDIX A: LOCAL APPROACH FOR A DIFFUSE INTERFACE

Following Ref. [48] we consider the scattering of the probe by a diffuse metallic interface, locally described by a position depending *local* dielectric function $\epsilon(x, \omega)$. In the standard dielectric formalism the probe scattering is due to the interaction of the probe $\rho_0(\mathbf{r}, \omega)$ with the induced potential $\phi_{\text{ind}}(\mathbf{r}, \omega)$. The induced potential can be calculated by removing the direct Coulomb field created by the probe from the total potential ϕ_{total} , which, in turn, can be calculated by solving the Poisson equation, $\nabla[\epsilon \nabla \phi_{\text{total}}] = 4\pi \rho_0(\mathbf{r}, \omega)$. Making use of the translational invariance on the YZ plane, we can recast the Poisson equation as an ordinary differential equation,

$$\left[\frac{d^2}{dx^2} + \frac{1}{\epsilon(x, \omega)} \frac{d\epsilon(x, \omega)}{dx} \frac{d}{dx} - q^2 \right] \phi_{\text{total}}(x, q_y, q_z, \omega) = -\frac{8\pi^2}{\epsilon(x, \omega)} \delta(x-b) \delta(q_z v - \omega), \quad (\text{A1})$$

where $q^2 = q_y^2 + q_z^2$ and q_y and q_z are the momentum components conjugate to the y and z coordinates. Because the factor $\delta(q_z v - \omega)$ in the RHT, the solution of the homogeneous equation can be written as a function of $Q = [q_y^2 + (\omega/v)^2]^{1/2}$. To build the solution of Eq. (A1), we numerically propagate its asymptotic regular solutions, $\phi_+(x, Q, \omega) = e^{-Qx}$ for $x > \max(b, h)$, and $\phi_-(x, Q, \omega) = e^{Qx}$ for $x < \min(b, -h)$, where h is the actual half thickness of the interface, up to the singularity at $x = b$. The continuity of the potential at this

point implies that the solution can be written as

$$\begin{aligned}\phi_{\text{total}}(x, q_y, q_z, \omega) \\ &= A(q_y, q_z, \omega)\phi_+(b, Q, \omega)\phi_-(x, Q, \omega), \quad x < b, \\ &= A(q_y, q_z, \omega)\phi_-(b, Q, \omega)\phi_+(x, Q, \omega), \quad x > b.\end{aligned}$$

The coefficient $A(q_y, q_z, \omega)$ is determined by the discontinuity of the derivative at the probe position,

$$A = -\frac{8\pi^2}{\epsilon(b, \omega)W(b, Q, \omega)}\delta(q_z v - \omega),$$

where $W(b, q, \omega)$ is the Wronskian,

$$\begin{aligned}W(x, Q, \omega) &= \phi_-(x, Q, \omega)\frac{d}{dx}\phi_+(x, Q, \omega) \\ &\quad - \phi_+(x, Q, \omega)\frac{d}{dx}\phi_-(x, Q, \omega),\end{aligned}$$

evaluated at $x = b$. The total potential $\phi_{\text{total}}(\mathbf{r}, t)$ is then defined piecewise,

$$\begin{aligned}\phi_{\text{total}}(\mathbf{r}, t) &= -\frac{1}{\pi v} \int d\omega dq_y \frac{\phi_-(b, Q, \omega)}{\epsilon(b, \omega)W(b, Q, \omega)} \phi_+(x, Q, \omega) \\ &\quad \times e^{iq_y y} e^{i(\omega/v)(z-vt)}, \quad x > b \\ &= -\frac{1}{\pi v} \int d\omega dq_y \frac{2\phi_+(b, Q, \omega)}{\epsilon(b, \omega)W(b, Q, \omega)} \phi_-(x, Q, \omega) \\ &\quad \times e^{iq_y y} e^{i(\omega/v)(z-vt)}, \quad x < b.\end{aligned}\quad (\text{A2})$$

The transverse force acting on the probe derives from the induced potential $F_x = -\partial_x \phi_{\text{ind}}(\mathbf{r}, t)$ evaluated at the probe position $\mathbf{r} = (b, 0, vt)$. To calculate the induced potential one has to remove from (A2) the field,

$$\phi_{\text{bulk}}(x, q, \omega) = \frac{4\pi^2}{\epsilon(b, \omega)} \frac{e^{-Q|x-b|}}{Q} \delta(q_z v - \omega), \quad (\text{A3})$$

which is the potential created by the screened probe in an unbounded medium of dielectric function $\epsilon(b, \omega)$. In doing so, we remove the singularity of ϕ_{total} at the probe position, and

the remaining potential $\phi_{\text{total}} - \phi_{\text{bulk}}$ represents the finite and continuous contributions of the interface. The contribution of ϕ_{bulk} is relevant to the calculation of the stopping power, but because of the isotropy on the XY plane its contribution to the transverse force is null. Then the transverse force acting on the probe is as follows:

$$F_x(b) = -\frac{2}{\pi v} \int_0^\infty d\omega \int_0^\infty dq_y \text{Re} \left[\frac{W(b, Q, \omega)}{\epsilon(b, \omega)} \right], \quad (\text{A4})$$

where Re stands for the real part of the argument.

APPENDIX B: THE CONSTITUTIVE RELATION

The CR which states the linearity between the polarizability \mathbf{P} , and the total electric-field \mathbf{E} through the susceptibility χ ,

$$\mathbf{P}(\mathbf{r}, \omega) = \int \chi(\mathbf{r}, \mathbf{r}', \omega) \mathbf{E}(\mathbf{r}', \omega) d\mathbf{r}', \quad (\text{B1})$$

or in the \mathbf{k} space,

$$P(\mathbf{k}, \omega) = \frac{1}{(2\pi)^3} \int \chi(\mathbf{k}, -\mathbf{q}, \omega) (\mathbf{q}, \omega) d\mathbf{q}, \quad (\text{B2})$$

can be recast as a scalar relation featuring the linearity of the response in terms of free (ρ_0) and induced (ρ) charge densities. This last magnitude is related to the polarization $\rho = -\nabla \cdot \mathbf{P}$ [49] so that

$$\rho(\mathbf{k}, \omega) = -\frac{i}{(2\pi)^3} \int \chi(\mathbf{k}, -\mathbf{q}, \omega) \mathbf{k} \cdot \mathbf{E}(\mathbf{q}, \omega) d\mathbf{q}. \quad (\text{B3})$$

The electric-field $\mathbf{E}(\mathbf{q}, \omega) = -\nabla \phi(\mathbf{q}, \omega)$, in turn, can be written in terms of the total charge density ρ_{tot} by means of the Gauss law $\phi(\mathbf{q}, \omega) = \frac{4\pi}{q^2} \rho_{\text{tot}}(\mathbf{q}, \omega)$. Finally,

$$\rho(\mathbf{k}, \omega) = -\frac{1}{2\pi^2} \int \frac{\mathbf{k}\mathbf{q}}{q^2} \chi(\mathbf{k}, -\mathbf{q}, \omega) \rho_{\text{tot}}(\mathbf{q}, \omega) d\mathbf{q}, \quad (\text{B4})$$

and after splitting ρ_{tot} into induced and free parts one gets Eq. (12).

-
- [1] E. Fermi, *Phys. Rev.* **57**, 485 (1940)
[2] R. H. Ritchie, *Phys. Rev.* **106**, 874 (1957)
[3] F. Ouyang and M. Isaacson, *Phil. Mag. B* **60**, 481 (1989); *Ultramicroscopy* **31**, 345 (1989).
[4] F. J. Garcıa de Abajo and J. Aizpurua, *Phys. Rev. B* **56**, 15873 (1997).
[5] F. J. Garcıa de Abajo and A. Howie, *Phys. Rev. Lett.* **80**, 5180 (1998).
[6] A. Rivacoba, N. Zabala, and J. Aizpurua, *Prog. Surf. Sci.* **65**, 1 (2000).
[7] F. J. Garcıa de Abajo, *Rev. Mod. Phys.* **82**, 209 (2010).
[8] J. M. Cowley, *Ultramicroscopy* **9**, 231 (1982); *Prog. Surf. Sci.* **21**, 209 (1986).
[9] A. Howie, *Ultramicroscopy* **11**, 141 (1983).
[10] P. M. Echenique and A. Howie, *Ultramicroscopy* **16**, 269 (1985).
[11] A. Rivacoba and P. M. Echenique, *Ultramicroscopy* **26**, 389 (1988).
[12] P. E. Batson, A. Reyes-Coronado, R. G. Barrera, A. Rivacoba, P. M. Echenique, and J. Aizpurua, *Nano Lett.* **11**, 3388 (2011).
[13] V. P. Oleshko and J. M. Howe, *Adv. Imaging Electron Phys.* **179**, 203 (2013).
[14] S. Gwo, H. Y. Chen, M. H. Lin, L. Sun, and X. Li, *Chem. Soc. Rev.* **45**, 5672 (2016).
[15] F. J. Garcıa de Abajo, *Phys. Rev. B* **70**, 115422 (2004).
[16] A. Reyes-Coronado, R. G. Barrera, P. E. Batson, P. M. Echenique, A. Rivacoba, and J. Aizpurua, *Phys. Rev. B* **82**, 235429 (2010).
[17] P. E. Batson, A. Reyes-Coronado, R. Barrera, A. Rivacoba, P. M. Echenique, and J. Aizpurua, *Ultramicroscopy* **123**, 50 (2012).
[18] M. J. Lagos, A. Reyes-Coronado, A. Konecna, P. M. Echenique, J. Aizpurua, and P. E. Batson, *Phys. Rev. B* **93**, 205440 (2016).
[19] J. Castrejon-Figueroa, J. . Castellanos-Reyes, and A. Reyes-Coronado, *Phys. Rev. B* **104**, 235416 (2021).
[20] N. D. Lang and W. Kohn, *Phys. Rev. B* **1**, 4555 (1970).

- [21] A. Rivacoba, *Ultramicroscopy* **207**, 112835 (2019).
- [22] J. Zuloaga, E. Prodan, and P. Nordlander, *Nano Lett.* **9**, 887 (2009).
- [23] J. Zuloaga, E. Prodan, and P. Nordlander, *ACS Nano* **4**, 5269 (2010).
- [24] A. Varas, P. García-González, J. Feist, F. J. García-Vidal, and A. Rubio, *Nanophotonics* **5**, 409 (2016).
- [25] W. Zhu, R. Esteban, A. G. Borisov, J. J. Baumberg, P. Nordlander, H. J. Lezec, J. Aizpurua, and K. B. Crozier, *Nat. Commun.* **7**, 11495 (2016).
- [26] M. Barbry, Ph.D. thesis, Basque Country University, 2018.
- [27] P. J. Feibelman, *Prog. Surf. Sci.* **12**, 287 (1982).
- [28] N. Asger Mortensen, P. A. D. Gonçalves, Fedor A. Shuklin, Joel D. Cox, C. Tserkezis, M. Ichikawa, and C. Wol, *Nanophotonics* **10**, 3647 (2021).
- [29] C. David and F. J. García de Abajo, *ACS Nano* **8**, 9558 (2014).
- [30] F. J. García de Abajo and P. M. Echenique, *Phys. Rev. B* **46**, 2663 (1992).
- [31] A. Rivacoba and N. Zabala, *New J. Phys.* **16**, 073048 (2014).
- [32] A. Reyes-Coronado, C. G. Ortíz-Solano, N. Zabala, A. Rivacoba, and R. Esquivel-Sirventl, *Ultramicroscopy* **192**, 80, (2018).
- [33] J. P. Muscat and D. M. Newns, *Surf. Sci.* **64**, 641 (1977).
- [34] R. H. Ritchie and A. L. Marusak, *Surf. Sci.* **4**, 234 (1966).
- [35] D. Wagner, *Z. Naturforsch. A: Phys. Sci.* **21**, 634 (1966).
- [36] N. Zabala and P. M. Echenique, *Ultramicroscopy* **32**, 327 (1990).
- [37] B. I. Lundqvist, *Physik Kondensierten Materie* **6**, 206 (1967).
- [38] A. D. Boardman, *Electromagnetic Surface Modes* (Wiley: New York, 1982).
- [39] R. H. Ritchie and A. Howie, *Philos. Mag. A* **58**, 753 (1988).
- [40] P. L. de Andres, P. M. Echenique, D. Niesner, T. Fauster, and A. Rivacoba, *New J. Phys.* **16**, 023012 (2014).
- [41] M. Urbieto, Ph. D. thesis, Basque Country University, 2021.
- [42] M. Abramowitz and I. A. Stegun, *Handbook of Mathematical Functions* (Dover, New York, 1964).
- [43] A. Howie and R. H. Milne, *Ultramicroscopy* **18**, 427 (1985).
- [44] A. Howie (private communication).
- [45] A. J. Bennett, *Phys. Rev. B* **1**, 203 (1970).
- [46] G. Chiarello, V. Formoso, A. Santaniello, E. Colavita, and L. Papagno, *Phys. Rev. B* **62**, 12676 (2000).
- [47] W. S. M. Werner, K. Glantschnig, and C. Ambrosch-Draxl, *J. Phys. Chem. Ref. Data* **38**, 1013 (2009).
- [48] A. Howie, F. J. García de Abajo and A. Rivacoba, *J. Phys. C* **20**, 304205 (2008).
- [49] J. D. Jackson, *Classical Electrodynamics* (Wiley, New York, 1975).